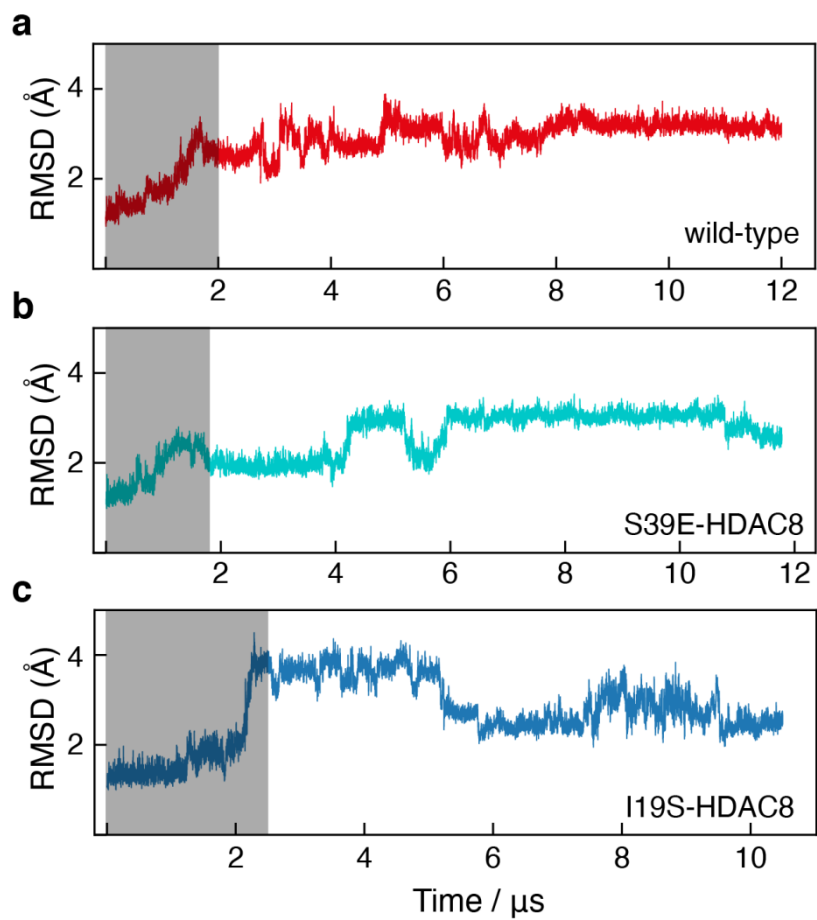


## Supplementary Materials for

### **Aromatic side-chain flips orchestrate the conformational sampling of functional loops in Human Histone Deacetylase 8**

Vaibhav Kumar Shukla, Lucas Siemons, Francesco L. Gervasio, D. Flemming Hansen\*

\*Corresponding author. Email: [d.hansen@ucl.ac.uk](mailto:d.hansen@ucl.ac.uk)



**Fig. S1.** Root-mean-square-deviation (r.m.s.d.) to starting structure for the three unbiased simulations. (a) RMSD for the wild-type simulation. A 2  $\mu$ s equilibrium time was chosen and 10  $\mu$ s production simulation (b) RMSD for the S39E-HDAC8 simulation. A 1.8  $\mu$ s equilibrium time was chosen leading to 10  $\mu$ s production simulation. (c) RMSD for the I19S-HDAC8 simulation. A 2.5  $\mu$ s equilibrium time was chosen followed by 8  $\mu$ s production simulation.

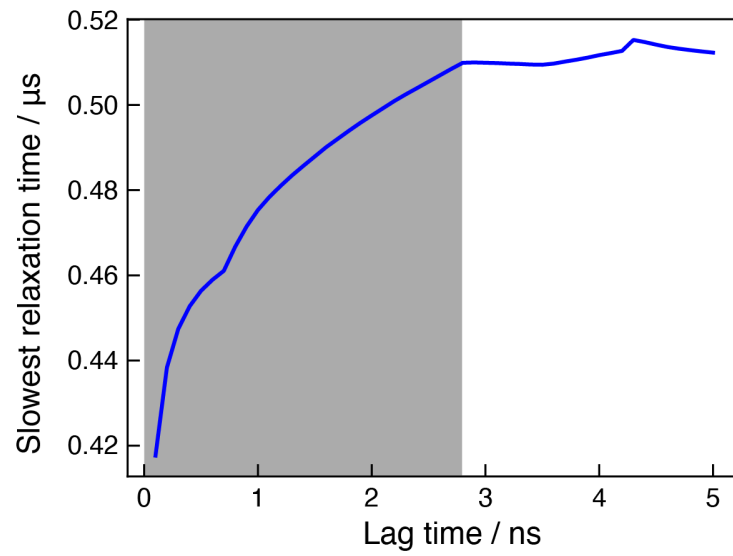


**Fig. S2.** Assessment of the convergence of the Markov state model. Shown is the slowest relaxation time of the transition matrix as a function of the lag time (see main text). The Markov state model is considered converged, when the slowest relaxation time becomes independent of lag time, that is 2.8 ns.

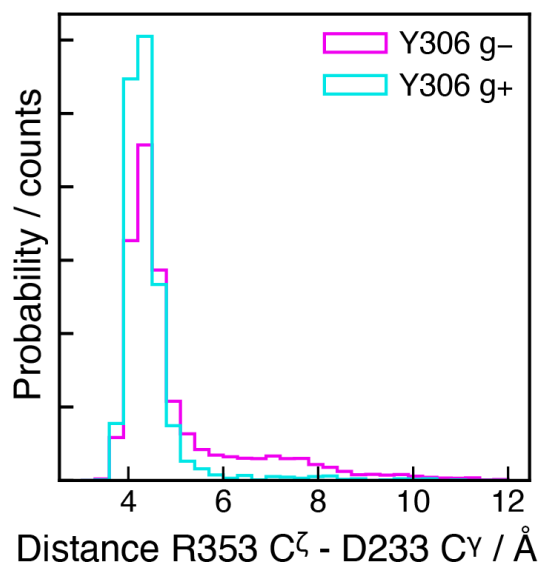


**Fig. S3.** Salt-bridge formation between R353 and D233. Probability distributions of salt bridge formation between R353 and D233 depending on the side-chain conformation of Y306. The salt bridge is fully formed, when the Y306 side-chain  $\chi_1$  angle is in the gauche+ (g+) conformation.

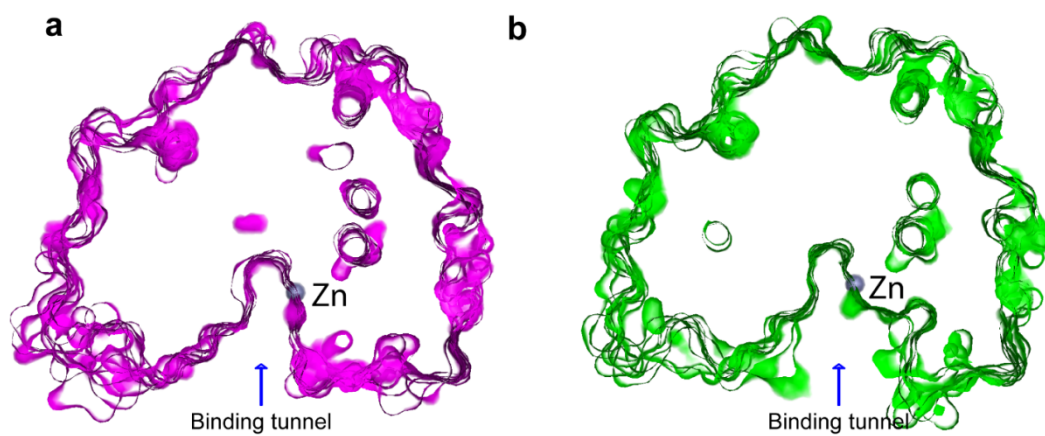


**Fig. S4.** Transition from Y306(g-) to Y306(g+) leads to an open state of the active site. (a) The cut-away surface views of ten random and representative structures of the substrate-binding tunnel in the Y306(g-) state. (b) The cut-away surface views of ten random and representative structures of the substrate-binding tunnel and active site in the Y306(g+) state, where the active site and substrate-binding tunnel are exposed to the bulk solvent.

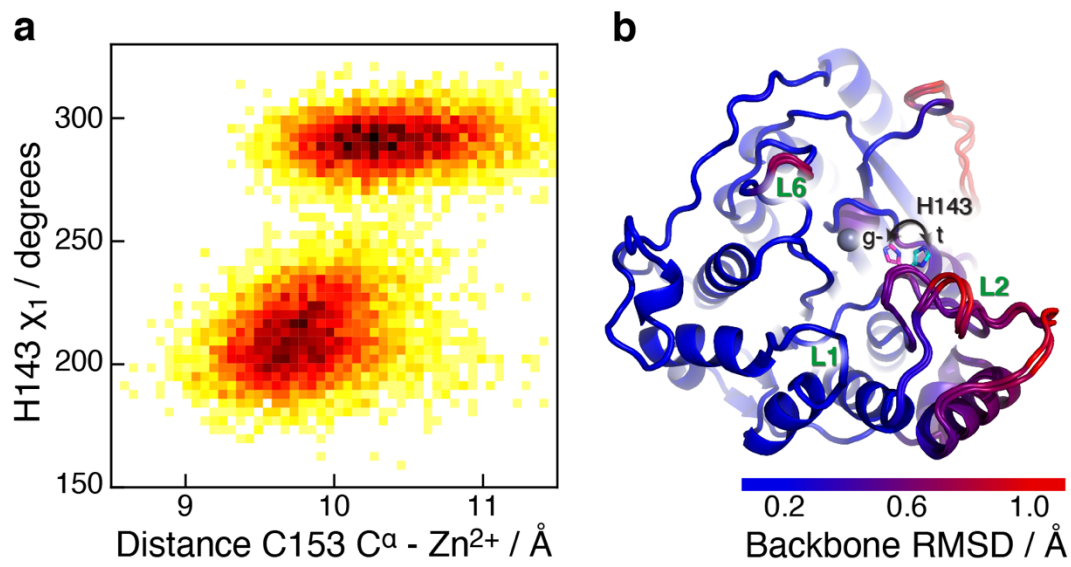


**Fig. S5.** Correlation between H143  $\chi_1$  and the conformation of loop L2. (a) The distance between C153 C $\alpha$  within the L3 loop region and Zn $^{2+}$  correlates with the  $\chi_1$  dihedral angle of H143. (b) The RMSD between the average H143(g-) and H143(t) conformations is shown. The  $\chi_1$  flip of H143 from *trans* to *gauche*- leads to the L2 region moving out and away from the active site by approximately 1 Å. The H143(g-) and H143(t) conformations are shown in magenta and cyan, respectively and the functional loops, L1, L2, and L6 labelled.

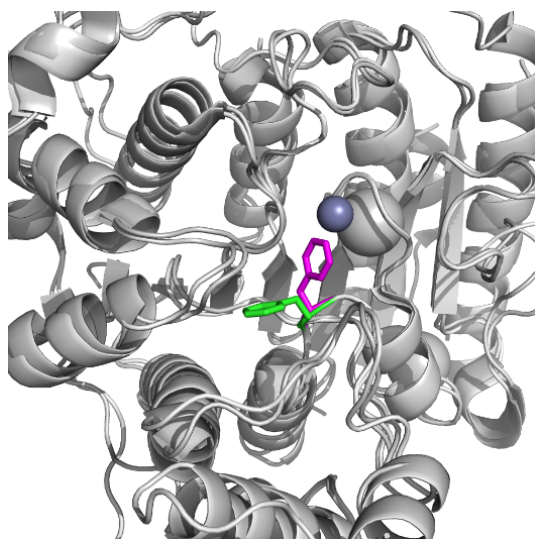


**Fig. S6.** Side-chain conformation of F152. Shown is residue F152 in human HDAC8 with  $\chi_1$  in *gauche*- (magenta; PDB: 1T69), and the corresponding F151 residue in the HDAC8 homologue from *Schistosoma mansoni* with  $\chi_1$  in *trans* (green; PDB: 6GXA).

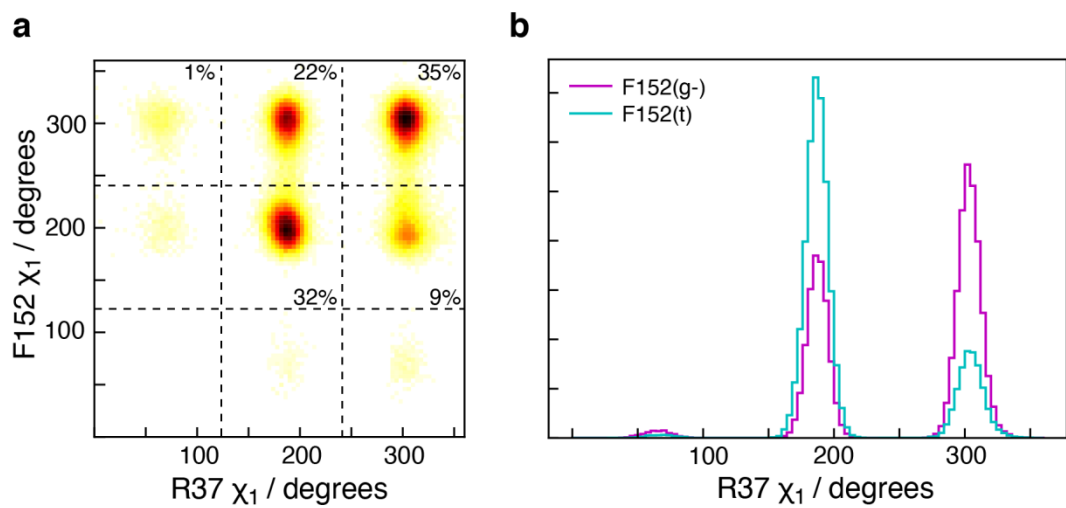


**Fig. S7.** Correlation between side-chain motions of F152 and R37. (a) Distribution of R37 and F152  $\chi_1$  dihedral angles. The  $\chi_1$  dihedral angle of F152 affects the sampling of R37; a residue which has been implicated in the release of the acetate product. (b) Histogram showing that the sampling of R37  $\chi_1$  depends on the  $\chi_1$  side-chain conformation of F152. When F152  $\chi_1$  is in a *trans* conformation the R37  $\chi_1$  angle is stabilised in the *trans* conformation.



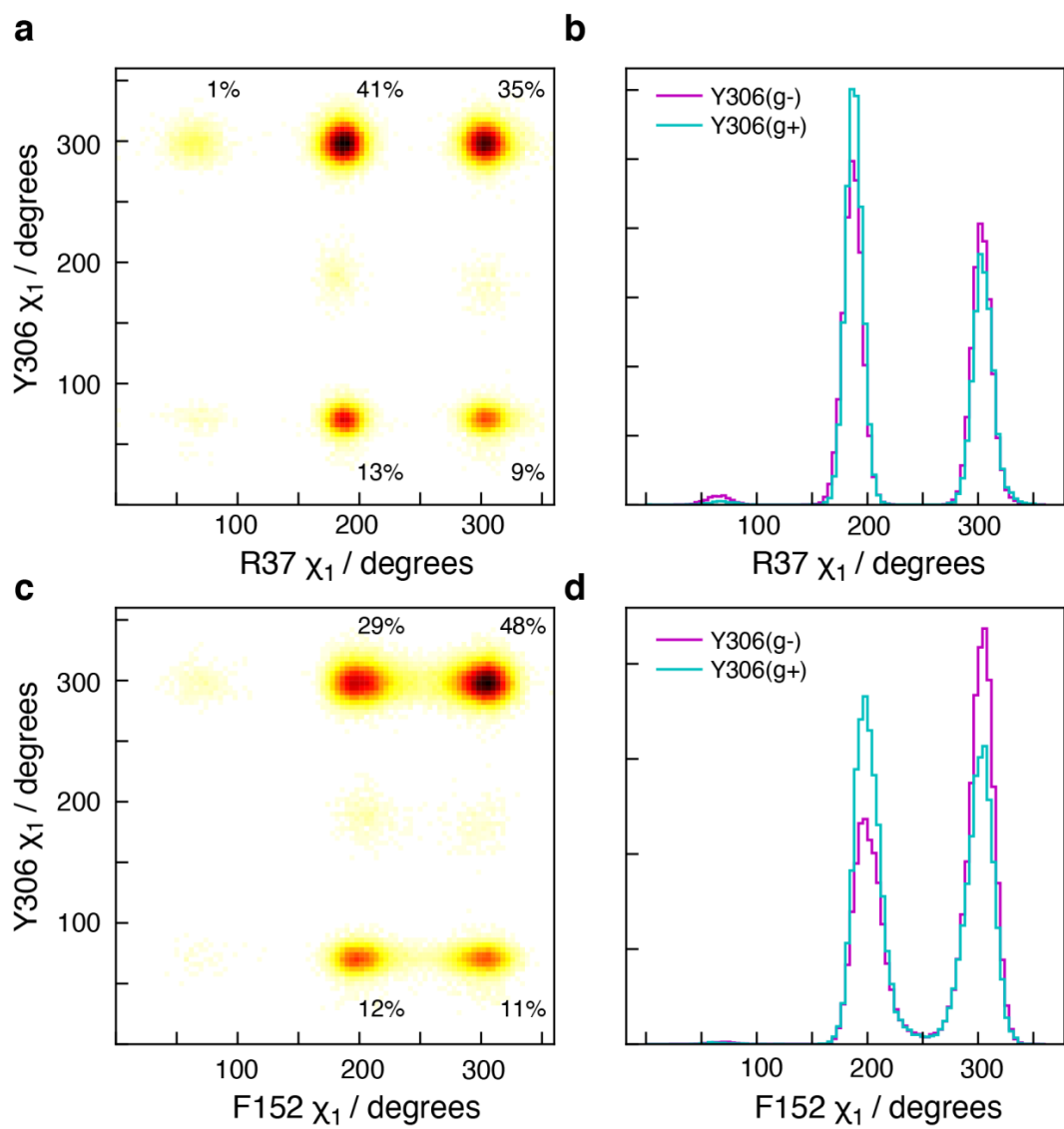


**Fig. S8.** Correlation between side-chain motions of Y306 and F152 and R37. (a) Two-dimensional histogram showing the combined distribution of R37 and Y306  $\chi_1$  dihedral angles. The  $\chi_1$  dihedral angle of Y306 shows minimal correlation with the sampling of R37. (b) Change in the sampling of R37  $\chi_1$ , depending on the side-chain conformation of Y306. (c) Two-dimensional histogram showing that the  $\chi_1$  dihedral angle of F152 is weakly correlated with the sampling Y306  $\chi_1$ . (d) Change in the sampling of F152  $\chi_1$ , depending on the side-chain conformation of Y306.

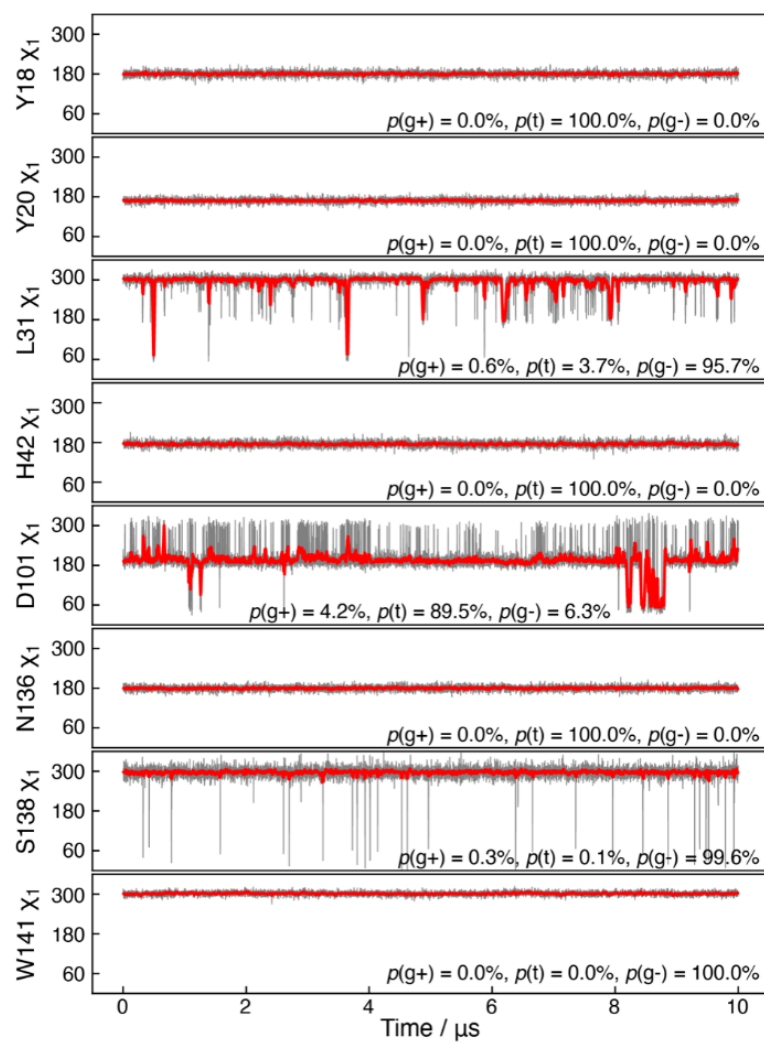


**Fig. S9.** Dihedral  $\chi_1$  angle for other residues. The  $\chi_1$  angle for residues Y18, Y20, L31, H42, D101, N136, S138, and W141, which are all located at the binding tunnel or the internal acetate release channel, as a function of simulation time (grey) and sampled every nanosecond. The red lines are moving averages over a window of 20 ns.

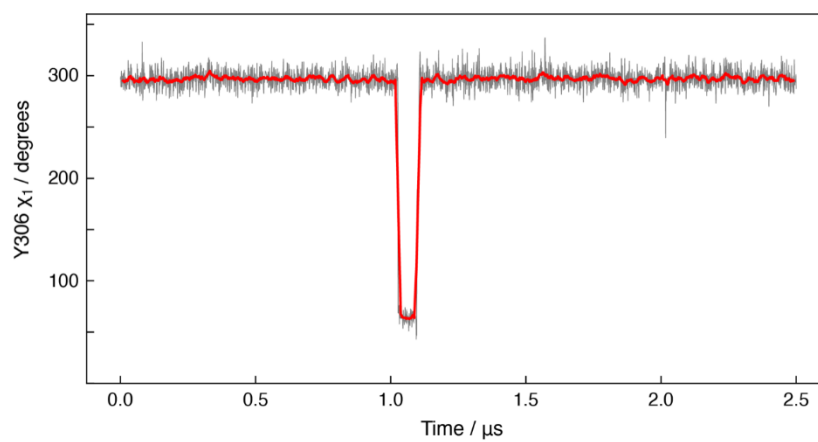


**Fig. S10.** Sampling of Y306 in the back-mutated S  $\rightarrow$  I mutation of the I19S-HDAC8 simulation. The Y306  $\chi_1$  angle as a function of simulation time (grey) and shown every nanosecond. The red line is a moving average over a window of 20 ns. As was seen in the initial simulation of wild-type HDAC8, two stable distinct conformation are observed, Y306(g-) and Y306(g+).

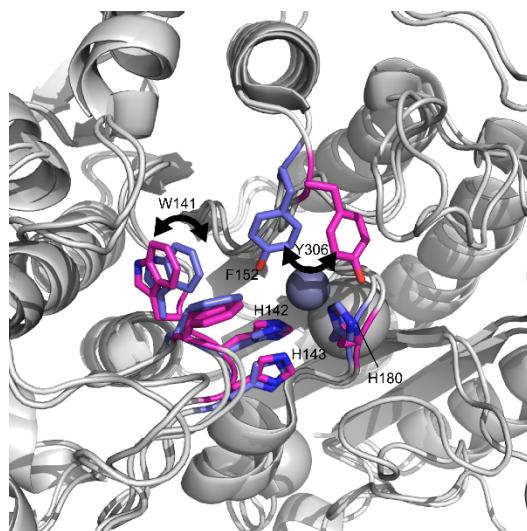


**Fig. S11.** Change in side-chain orientation of various residues in the bound- to apo-state transition. Side chains of the residues in the “apo-state” and in the “bound-state” are shown in magenta and blue colour, respectively.